ARTICLE

Hyper-fast gas chromatography and single-photon ionisation time-of-flight mass spectrometry with integrated electric modulator-based sampling for headspace and on-line VOC analysis

Received 00th January 20xx,
Accepted 00th January 20xx

DOI: 10.1039/x0xx00000x

Christian Gehm,[a] Kevin Schnepel,[a] Hendryk Czech,*[a,b] Toni Miersch,[a] Sven Ehlert[c] and Ralf Zimmermann[a,b]

We developed a novel fast gas chromatography (fastGC) instrument with integrated sampling of volatile organic compounds (VOCs) and detection by single-photon ionisation (SPI) time-of-flight mass spectrometry (TOFMS). A consumable-free electric modulator rapidly cools down to -55°C to trap VOCs and inject them on a short chromatographic column by prompt heating to 300°C, followed by a carrier gas exchange from air to helium. Due to the low thermal mass and optical heating, the fastGC is operated with in total runtimes incl. cooling of 30 s and 15 s, referring to hyper-fast GC, and a constantly increasing temperature ramp from 30°C to 280°C. The application of soft SPI-TOFMS allows detecting of co-eluting VOCs of different molecular composition, which cannot be resolved be conventional GC (cGC) with electron ionisation (EI). Among other analytical figures of merit, we achieved limits of detection for toluene and *p*-xylene of 2 ppb and 0.5 ppb, respectively, at a signal-to-noise ratio of 3 and linear response over a range of more than five orders of magnitude. Furthermore, we demonstrate the performance of the instrument on samples from the fields of environmental research and food science by headspace analysis of roasted coffee beans and needles from coniferous trees as well as by quasi-real-time analysis of biomass burning emissions and coffee roast gas.

Introduction

Direct inlet mass spectrometry (DI-MS) is a powerful method for on-line analyses of volatile organic compounds (VOCs) when high time resolution is required or in headspace analysis. In particular soft ionisation techniques, such as single-photon ionisation (SPI) and resonance-enhanced-multiphoton ionisation (REMPI)[1], proton-transfer reaction (PTR), secondary ion flowtube ionisation (SIFT) as well as chemical ionisation under vacuum (CI) or atmospheric pressure (APCI)[2], generate predominantly molecular and quasi-molecular ions, showing advantages compared with fragmenting “hard” electron ionisation (EI) as it increases the interpretability of mass spectra. However, despite the possibility of using mass analysers with high resolution, isomers cannot be individually detected. Thermal desorption or liquid injection gas chromatography (GC) is able to separate isomeric compounds, but with the cost of losing time resolution of the measurement. Additionally, it requires labour-intensive offline sampling, e.g. on adsorbent tubes, passivated stainless steel canisters or in gas sampling bags, which may be supported by cryogenic trapping, and subsequent sample preparation, such as solid phase microextraction[3]. Moreover, VOCs may undergo significant degradation when adsorbed and exposed to atmospheric oxidants during sampling[4]. For the on-line analysis of VOCs in tobacco smoke, a heated sample loop was successfully used, however, because of limitations in GC operation, the method had an upper limit in analyte volatility equal to that of toluene[5]. A portable GC instrument with sensor array detection was reported deploying a multi-stage adsorbent consisting of Carbopack B, Carbopack X and Carboxen 1000 for preconcentration with integrated injection module with resistively heating, but with limitations to compounds having vapour pressures above 0.4 torr[6].

GC analysis can be divided based on its runtime and separates to conventional GC (cGC; runtime >20 min) from fast GC (3-20 min), very-fast GC (1-3 min), hyper-fast GC (1-60 s) and ultra-fast GC (<1 s)[7]. Starting from cGC, reduced GC runtimes may be achieved by different strategies, for example by simply shortening column length or increasing the capillary inner diameter[7] leading to lower peak capacity, plate number and height. Additionally, the GC run is often limited to isothermal conditions or less dynamic temperature programmes because of the time limitations. A unique fastGC approach was recently described with the extension of fast GC to two-dimensional fast GC, substantially increasing separation performance while keeping the total GC runtime below 20 min[8].

The addition of fast gas chromatography with runtimes below 20 min (fastGC) to different mass analysers offers a compromise

[a] Joint Mass Spectrometry Centre, Chair of Analytical Chemistry, University of Rostock, 18059 Rostock, Germany
email: hendryk.czech@uni-rostock.de
[b] Joint Mass Spectrometry Centre, Cooperation Group “Comprehensive Molecular Analytics” (CMA), Helmholtz Zentrum München, 81379 München, Germany
[c] Photonion GmbH, 19061 Schwerin, Germany

† Electronic Supplementary Information (ESI) available: [details of any supplementary information available should be included here]. See DOI: 10.1039/x0xx00000x

between chemical specificity and time resolution. Often a baseline separation of two analytes is not necessary that the benefit from shorter time of analysis prevails. Such fastGC methods have been described for the analysis of samples from various fields, for example tobacco smoke by SPI[5], monoterpenes from plants by SIFT[9], doping control by GC combustion isotope ratio MS[10], flame retardants by atmospheric pressure photoionisation (APPI)[11] or whole-body, dermal and breath VOC emission from humans by PTR[12].

The setup of this study comprises of individual devices to perform convenient VOC sampling and a rapid temperature programme to increase the chemical space of VOC detection compared to DI-MS in targeted and untargeted headspace and on-line analysis of complex mixtures and dynamic processes. An electric consumable-free modulator with two stages rapidly cools down to -55°C and heats up to 300°C in order to trap and release VOCs on a GC column[13]. Additionally, an optically heated GC enables fast temperature programmes within GC runtimes of 30 s with maximum heating rates and cooling rates of 10.0 K s^{-1} and 50 K s^{-1}, respectively[14]. After successful application of the optically heated GC with cryogenic sampling of VOCs evolving from the simulation of nut roasting in thermal gravimetric analysis[15], we present headspace and on-line measurements of environmental and food samples with carrier gas exchange to helium for rapid analysis with advanced chemical speciation of VOCs by hyper-fast GC-SPI time of-flight mass spectrometry (TOFMS) for quasi-real-time monitoring.

Experimental

Materials, chemicals and samples

Analytical figures of merit were obtained from the analysis of a gas standard consisting of toluene and *p*-xylene in a pressure vessel filled with nitrogen. The true concentration was obtained from comparing the measured intensities with the intensities from a calibration gas standard (BTXT) of either 10 ppm or 1 ppm of in nitrogen 5.0 (benzene, toluene, *p*-xylene and 1,2,4-trimethylbenzene (TMB); Linde AG, Munich, Germany). Additionally, a standard solution of eight monoterpenes containing α-pinene, β-pinene (99% purity, Sigma Aldrich, Merck KGaA, Darmstadt, Germany), Δ-3-carene (90% purity, TCI-Tokyo Chemical Industry Co., LTD., Tokyo, Japan), α-terpinene, camphene (95% purity, Sigma Aldrich, Merck KGaA, Darmstadt, Germany), limonene, γ-terpinene (95% purity, TCI-Tokyo Chemical Industry Co., LTD., Tokyo, Japan), and myrcene (technical grade, Sigma Aldrich, Merck KGaA, Darmstadt, Germany) was prepared in methanol (99.9% purity, ROTISOLV® HPLC Gradient, Carl Roth GmbH + Co. KG, Germany).

Pine needles on small twigs of black pine (*Pinus nigra*) and Serbian spruce (*Picea omorika*) were collected at suburban sites of Rostock, Germany. Branches and twigs of Scots pine (*Pinus sylvestris*) and common oak (*Quercus robur*) from freshly cut branches were stored for two weeks in a dry place at room temperature and burned with a batch size of approximately 2.0 kg in an open fireplace.

Green coffee beans of Arabica coffee from Brazil (*Santos*) and Colombia (*Excelsior*) and one Robusta coffee from Vietnam (*Grade 3*) were roasted in a drum roaster (*Probatino, PROBAT-Werke von Gimborn Maschinenfabrik GmbH, Emmerich am Rhein, Germany*; batch size of 1.5 kg) to a medium-dark roast degrees, determined by a reflectance measurement

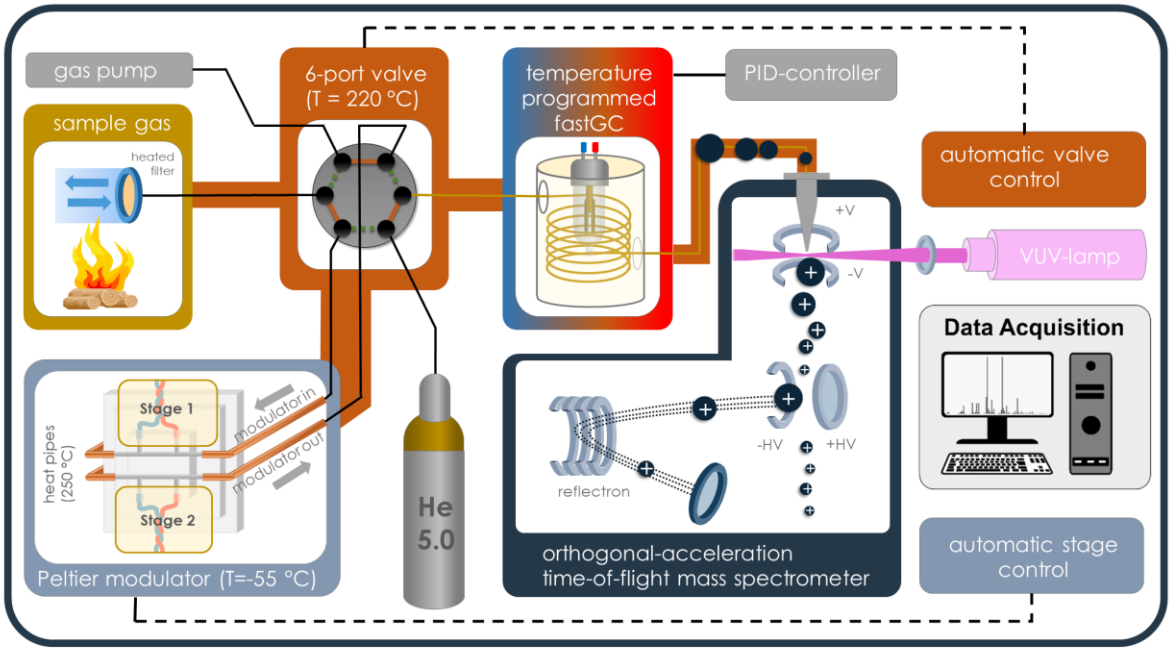

Fig. 1 Schematic setup of the fastGC-SPI-TOFMS system in "sampling" mode for headspace analysis of needles with sampling unit, 6-port-2-way valve for changing to helium as GC carrier gas, electric modulator, optically heated fastGC, VUV-lamp for SPI and orthogonal-acceleration TOFMS.

(*Colorette 3b*, PROBAT-Werke von Gimborn Maschinenfabrik, Emmerich am Rhein, Germany).

Instrumentation

The instrumental setup consists of an electrical 2-stage modulator[13], an optically heated fastGC[14], an orthogonal acceleration time-of-flight mass spectrometer (oa-TOFMS; Tofwerk AG, Thun, Switzerland; 1,300 time-of-flight resolution at m/z 92), a deuterium VUV-lamp for ionisation (L2D2 lamp L7293, Hamamatsu Photonics K. K., Japan; spectral distribution from 115 nm to 400 nm, VUV peak emission at 126 nm and 122 nm) and a heated 2-way-6-port valve (Valco Instruments Inc., Houston, TX) (Fig. 1). VOCs were sampled, either directly or from a headspace container (volume of 20 ml, clear glass), through a heated deactivated transfer capillary (Restek MXT Gurad Column, ID of 530 µm, 2 m length, BGB Analytik Vertrieb GmbH; heated to 205°C) and trapped on a GC-column (HT-5, SGE Analytical Science Ltd.; ID 250 µm, film thickness 0.1 µm) inside the modulator, which is cooled to -55 °C in sampling mode. Subsequently, the sample was transferred from the modulator stage into the optically heated fastGC unit with 3 m GC column length by rapid temperature increase. At the same time, the 2-way-6-port valve changed its position from "sampling" to "GC", providing helium as carrier gas. Eluents from fastGC separation over the GC column with a temperature ramp from 30°C to 280°C (equal to a temperature ramp of 10 K s^{-1}) were ionised by SPI with VUV-photons from the deuterium lamp. The mode of photon energies from the deuterium lamp appears in the range of common ionisation energies for organic molecules and principally all compounds with ionisation energies below 10.78 eV, equal to the lower emission wavelength limit of 115 nm, may be ionised, but with different ion yields. Consequently, the low amount of excess energy received by a molecule cause only minor fragmentation[1]. Finally, the ions were detected by the oa-TOFMS with an ion extraction frequency of 70,000 Hz and a data acquisition rate of 20 Hz. Thus, 3500 individual spectra were accumulated to generate one mass spectrum with a resulting time resolution of 50 ms. After the chromatographic run of 25 s, the fastGC column is cooled by blowing room air for 5 s becoming enabled to repeat the procedure. Hence, we sort our fastGC analysis to the class of hyper-fast GC.

Sampling and settings in headspace and on-line analysis

Headspace analysis needles and coffee beans was conducted in a glass container with a volume of 20 cm^3, which was provided with a hole of 0.5 mm for equilibrium to avoid under pressure caused by the sampling flow of approximately 4 ml min^{-1} with 2-way-6-port-valve in position "sampling" (20 ml min^{-1} in valve position "GC" during desorption) . On-line analyses of hot gases from coffee roasting or biomass burning were performed from a heated sampling line with 4 mm inner diameter, consisting of stainless steel, which was heated to 180°C.

We found that compounds at the upper limit of the VOC range sampled from hot exhaust gas of coffee roasting and biomass burning were inefficiently released from the modulator and did not appear as peaks in the chromatogram. Therefore, we increased the time for injecting trapped compounds from the modulator into the GC to 15 s. However, this benefit of increased volatility range for analytes was achieved by the cost of missing sampling time. In headspace analyses at room temperature and calibration gas measurements, the analyte volatility range has a lower ceiling, so the effect of longer injection time was small. However, for comparison purposes, all measurements were done with the same modulator settings except on-line measurements at the coffee roaster because of high concentrations and higher required time resolution. To gain the necessary time resolution for coffee roast gas analysis, we shortened the GC cycle to 15 s with 3 s of modulator sampling and a GC runtime of 12 s with the same start and end temperature, thus increasing the temperature ramp by a factor of 2 compared to the other measurements.

Data analysis

Data processing and analysis was performed in MATLAB (version 2018; The MathWorks Inc., Natick, MA) by self-developed processing routines and Matlab's Statistics Toolbox for non-negative matrix factorisation (NMF). For deconvolution purposes, NMF was applied with a combined multiplicative update algorithm for initial value optimisation followed by alternating least-square algorithm[16] with a maximum number of 20 iterations in each of the 100 performed replicates.

Results and discussion

Analytical figures of merit

The following figures of merits were determined with the calibration gas standard and comprises the trapping efficiency of the modulator, limit of detection (LOD), linearity and dynamic range related to the mass spectrometric detection, and reproducibility of the chromatographic separation (Fig. 2).

Trapping efficiency. We assessed the trapping efficiency of the four standard gas constituents by relating the analyte intensities of 36 consecutive chromatograms to the cumulative intensities for each analyte after direct inlet of the standard gas into the oa-TOFMS for 15 s. For BTXT we obtained trapping efficiencies of 10%, 22%, 74% and 78%, respectively. These results are specific for the applied GC column and time of the sampling mode. Different polarity and film thickness of the GC column material may alter the trapping efficiency and may be adjusted for targeted analysis of analytes. Moreover, after injection of the trapped VOCs at 300°C, the second stage of the modulator requires about 11 s to asymptotically reach the final sampling temperature of -55°C, however, only 3.7 s to reach -40°C[13]. Hence, moderately longer times in sampling mode will likely increase the trapping efficiency.

LOD, precision, linearity and dynamic range. The LOD was determined with two common approaches. First, we calculated baseline mean intensity and the standard deviation (σ) of the noise at the molecular masses of toluene and *p*-xylene. The critical peak height related to the LOD is obtained from

$$Int_{crit} = \overline{baseline} + 3\sigma \qquad (1)$$

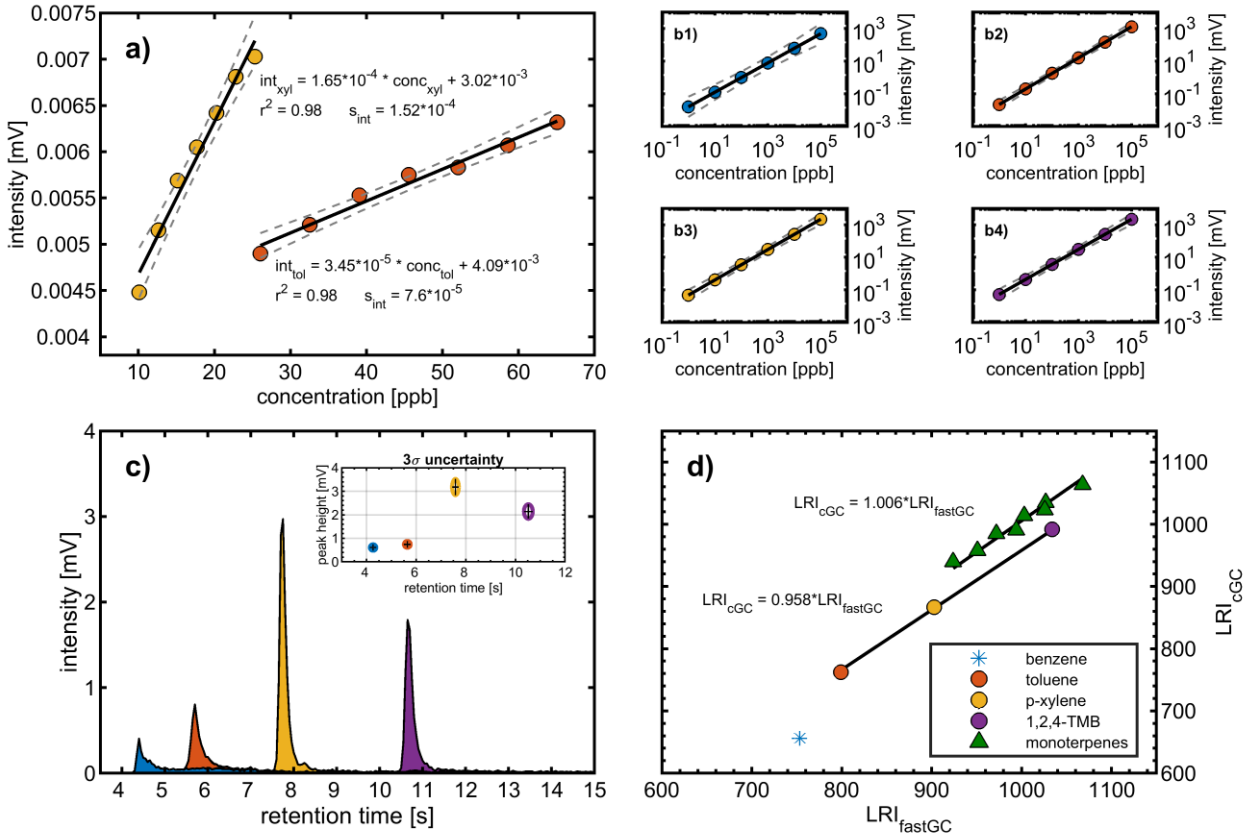

Fig. 2 Analytical figures of merit comprising a) calibration functions of toluene (T) and *p*-xylene (X) with coefficient of determination r^2 and residual standard deviation s_{int}, b1-b4) linearity over five orders of magnitude, c) peak shape and precision (3 σ) of intensity and retention time from repeated BTXT analysis, and d) comparison of LRI obtained from fastGC with LRI obtained from cGC for BTXT and 8 monoterpenes.

which is set in relation to the standard gas of 1 ppm. From 10 consecutive chromatograms, we obtain 2 ppb for toluene and 0.5 ppb for *p*-xylene, which is competitive with LODs from previously published fastGC setups with soft ionization mass spectrometry[9,17,18] or fast GC with sensor array detection[6] for analytes of similar volatility.

It has been found that the photoionisation cross section at 126 nm of *p*-xylene differs by less than 25% of the one of toluene[19], we attribute the lower LOD of p-xylene to the higher trapping efficiency.

In the second approach, we created a calibration function starting with six calibration standards of one order of magnitude higher concentrations than the LOD determined based on blank values (LOD_{blank}). Similarly, each data point was generated from 10 consecutive chromatograms and the resulting linear regression had a coefficient of determination >0.98 for both calibration functions (Fig. 2a). We obtain LODs from the calibration functions (LOD_{cfun}) of 7.1 ppb and 3.0 ppb for toluene and *p*-xylene, respectively, which are about a factor of 4 higher than LOD_{blank}. The LOD_{cfun} is directly related to the goodness of the calibration function and the selected parameters, such as distance between the concentrations. From the repeated analyses of 1 ppm of BTXT, we assessed a mean relative measurement uncertainty of 15% (3σ of 36 chromatograms) (Fig. 2c), which is close to the distance between the concentrations causing larger confidence bands and consequently higher LOD_{cfun}.

The linearity and dynamic range of the fastGC setup was evaluated with six concentrations standards of 1 ppb to 100 ppm of BTXT prepared in methanol, which was injected using a nebuliser system[20]. From the log-log-presentation of the data, we obtained coefficients of determination of 0.97 for benzene and >0.99 for toluene, *p*-xylene and TMB. Furthermore, the peak intensity at 100 ppm approaches the upper limit of the measurement channel. The dynamic range of an instrument is defined as the ratio of this upper measurement limit and the LOD[21]. Hence, the fastGC setup gives a linear response with increasing concentrations over more than five orders of magnitude (Fig. 2b).

Retention time precision and peak shape. The precision and repeatability of the retention time is crucial for the identification of chromatographic peaks, e.g. by the retention index by Kovats[22] for isothermal GC or van den Dool and Kratz for temperature-programmed GC runs[23]. From 36 consecutive chromatograms, we obtain a standard deviation of the retention times from 43 ms to 59 ms, which is equal to a relative precision of 1% (for benzene) to 0.6% (for *p*-xylene and TMB) (Fig. 2c) and competitive with a previously reported fastGC setup[17].

The peak shapes were evaluated by the symmetry coefficient S. For this purpose, we drop a perpendicular from the maximum peak height and consider the distances of this perpendicular to the peak on the left (B) and right hand side (A) at 10% peak height:

$$S = \frac{B_{10\%}}{A_{10\%}} \qquad (2)$$

Therefore, S>1 denotes peak tailing and S<1 denotes peak fronting. For the aromatic compounds of BTXT, there is a tendency towards tailing eluents confirmed by S values from 5.5 (benzene) to 2.4 (TMB) at concentrations in the centre of the dynamic range (Fig. 2c). We attribute this behaviour to relatively strong interactions between the GC column material inside the modulator and the p-orbitals of the aromatic π-systems since the symmetry coefficient S of aliphatic compounds, such as monoterpenes, approaches unity (Fig. 3 bottom).

Applicability of the linear retention index (LRI). The linear retention index (LRI) of van den Dool and Kratz[23] enables identification of analytes based on their retention times relative to the homologous series of n-alkanes. In contrast to the original index by Kovats[22], LRI is appropriate for GC runs with a temperature-gradient and calculated as following

$$LRI = 100 \cdot \left[n + \frac{RT_u - RT_n}{RT_{n+1} - RT_n}\right] \qquad (3)$$

with RT being the retention times of the unknown species u, the n-alkane with n carbons atoms eluting before the unknown species and the n-alkane n+1 eluting after the unknown species. Our n-alkane standard ranged from n-octane to n-tridecane, covering retention times from 5.66 s to 18.13 s. In order to calculate LRI for benzene and toluene, the RT was extrapolated to n-hexane (Fig. S1).

For BTXT, we obtained a limited agreement between LRI from Lai et al. (1995)[24] and our measurements (Fig. 2d). In particular for benzene having the highest volatility of all analytes, LRI from our measurements exceeds the LRI from cGC of 656 by 99, which is distinctly higher than the suggested maximum different of 1%[25]. Other constituents of BTXT have also higher LRI than reported in the literature, but with an almost constant positive bias of 4.4% and consequently high correlation (without benzene $r^2 = 0.999$; including benzene: $r^2 = 0.910$). In the data of Lai et al. (1995)[24], it is evident that increasing the temperature ramp of the GC run increases the LRI, so substantially higher LRIs at a temperature ramp of 600 °C min^{-1} in our measurements are reasonable. For the case of benzene, the LRI additionally suffers from increased uncertainty because of extrapolated and very low retention time with associated high uncertainty of $RT_{n\text{-hexane}}$. In order to further explore this issue, we investigated the behaviour of the compound class of monoterpenes, which cover boiling points within the range of BTXT, regarding their LRIs and compared them to previously reported LRI[26]. In fact, the agreement for this compound class was substantially better than for BTXT with differences in LRI of less than 1 % for all monoterpenes except α-pinene, β-pinene and Δ-3-carene (Fig. 2d). Therefore, the suitability of LRIs from different temperature programmes for compound identification in fastGC analysis may differ between compound classes and volatilities. However, the order of eluting monoterpenes followed according to the LRI determined by cGC. Moreover, we run a Monte Carlo simulation of 1000 repetitions for limonene, eluting between n-decane and n-undecane, to estimate the uncertainty of its LRI in fastGC based on the uncertainty in retention time we obtained from 36 chromatograms. The resulting root mean squared error (RMSE) of ±2.7 is distinct
higher than the general uncertainty in LRI for cGC of ±2 or 1% of LRI_{cGC} [24,25], but may still be useful for compound identification if a database for typical temperature-programmed fastGC is available.

Headspace analysis

Measurements with the fastGC setup was conducted for two common applications from the field of environmental chemistry and food science. Rapid measurements in headspace analysis with fastGC may open the possibility of high-throughput screening of multiple samples and enables to analyse dynamic VOC composition in case of a static experiment setup with changing experimental conditions.

Monoterpenes in conifer needles. On a global scale, VOC emissions from plants are the most relevant precursors for the formation of secondary organic aerosol (SOA) in the atmosphere with effects on climate and human health[27]. Monoterpenes constitute one of the most abundant plant emissions and give an indication of poor health condition of an individual tree or an entire forest caused by insect infestation or draught stress[28]. Moreover, SOA from the photooxidation of α-pinene has been shown to contain significant amounts of reactive oxygen species, inducing oxidative stress and a reduce viability in cell exposure[29].

We started our targeted analysis with a mixture of eight individual monoterpenes to obtain their retention times and mass spectra (Fig. 3). The chromatogram was built-up from two monoterpene standards with alternating retention times in order to attain information on the pure substances, but also to illustrate the situation in a measurement of a real sample.

Despite generally fragment-poor ionisation, the base peaks in mass spectra of rather labile α-pinene, β-pinene and myrcene did not appear as molecular ions at m/z 136. The main fragments we observed were m/z 80, m/z 92, m/z 93, m/z 94, m/z 107 and m/z 121, which exceeded the intensity of the molecular ion for all monoterpenes except for α-terpinene, γ-terpinene and limonene. With the applied temperature settings, all monoterpenes eluted between retention times of 8 s and 13 s (Fig. 3). In order to keep the analysis time short, we approve the poor separation of myrcene and Δ-3-carene as well as α-terpinene and limonene with a chromatographic resolution of 0.52 and less than 0.05, respectively. Although not baseline-resolved, myrcene and Δ-3-carene may be distinguished by their characteristic fragmentation patterns. For the separation problem of α-terpinene and limonene, we exploited those differences by 100 runs of the NMF procedure described in the section on data analysis with a two-factor solution in order to

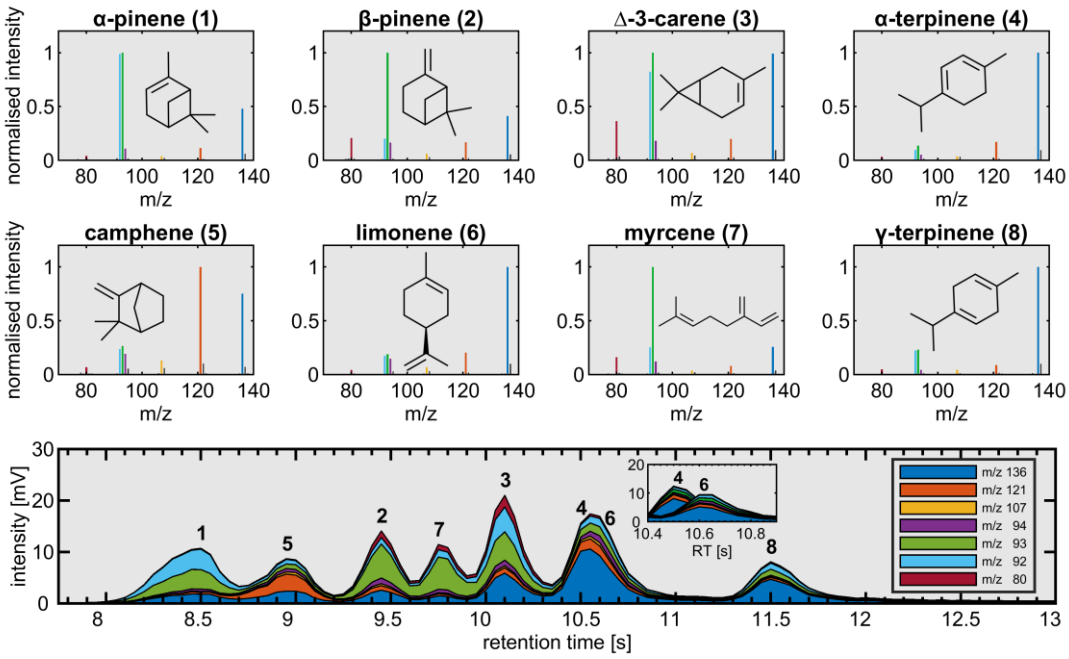

Fig. 4 SPI mass spectra of eight individual monoterpenes (top) and chromatogram of the monoterpene mixture (bottom). The overlapping peaks of α-terpinene (4) and limonene (6) are deconvolved by non-negative matrix factorization (NMF) due to slight differences in fragmentation with monoterpene-related fragments highlighted in colours.

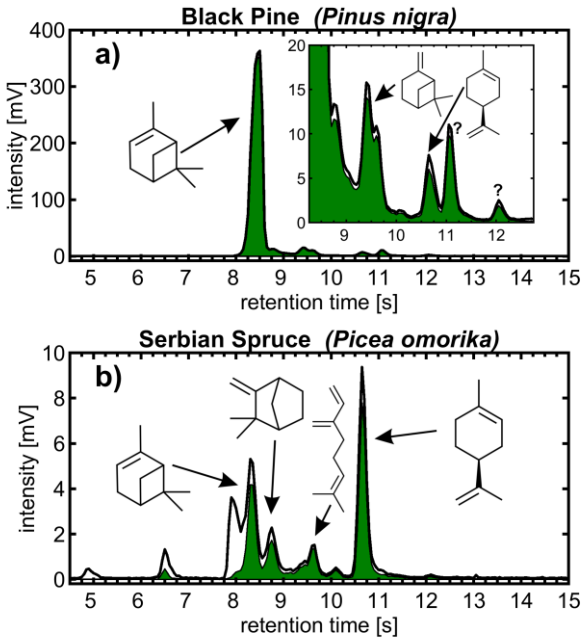

Fig. 3 Chromatogram of headspace analysis of needles from a) black pine and b) Serbian spruce. The black line denotes the total ion intensity, while the green area represents monoterpene-related ion intensities m/z 80, 92, 93, 94, 107, 121, and the molecular ion at m/z 136.

deconvolve the unresolved chromatographic peak. The mean result of NMF outputs gave two distinct peaks having uncentred correlation coefficients of >0.97 with the mass spectra of pure α-terpinene and limonene, respectively (Fig. 3 bottom).

Needles of black pine and Serbian spruce from the pine family *Pinaceae* were selected as real samples for headspace analysis of natural monoterpene emissions. All monoterpenes were identified based on their retention time at peak height within a tolerance of 0.1 s and uncentred correlation coefficient of the mass spectrum with the pure monoterpene of >0.9. In particular for black pine, monoterpene emissions were strongly dominated by α-pinene[30], accounting for 88% of the total peak height associated with m/z from monoterpenes (Fig. 4a). Furthermore, β-pinene, myrcene, limonene, Δ-3-carene and, despite high interfering peak of α-pinene, also camphene were detected together with two unknown peaks with retention times at 11.05 s and 12.05 s. Peaks of retention times beyond the eight targeted monoterpenes showed highest correlations with the fragment-poor mass spectra of α-terpinene, γ-terpene and limonene. Thus, the mass spectral signature points toward a monocyclic monoterpene with a menthane backbone, which is likely β-phellandrene when additionally considering its LRI between limonene and γ-terpinene as well as its general abundance in black pine needles[30].The peak at retention time 12.05 s shows a clear contribution from the molecular monoterpene ion at m/z 136, but more substantial fragmentation, giving indication for an aliphatic or bicyclic monoterpene species.

We could detect almost the same monoterpenes for needles of Serbian spruce (Fig. 4b) as for black pine, but with more equally distributed concentrations. The highest peaks eluting at 10.65 s and 8.35 s can be attributed to limonene and α-pinene, followed by minor contributions of camphene, myrcene and Δ-3-carene.

Considering fastGC-SPI-TOFMS as an untargeted analysis, also other emissions from conifer needles could be detected, such as VOCs of higher or similar volatility as monoterpenes indicated by the difference between monoterpene-related and total peak intensity, which is in particular pronounced for short

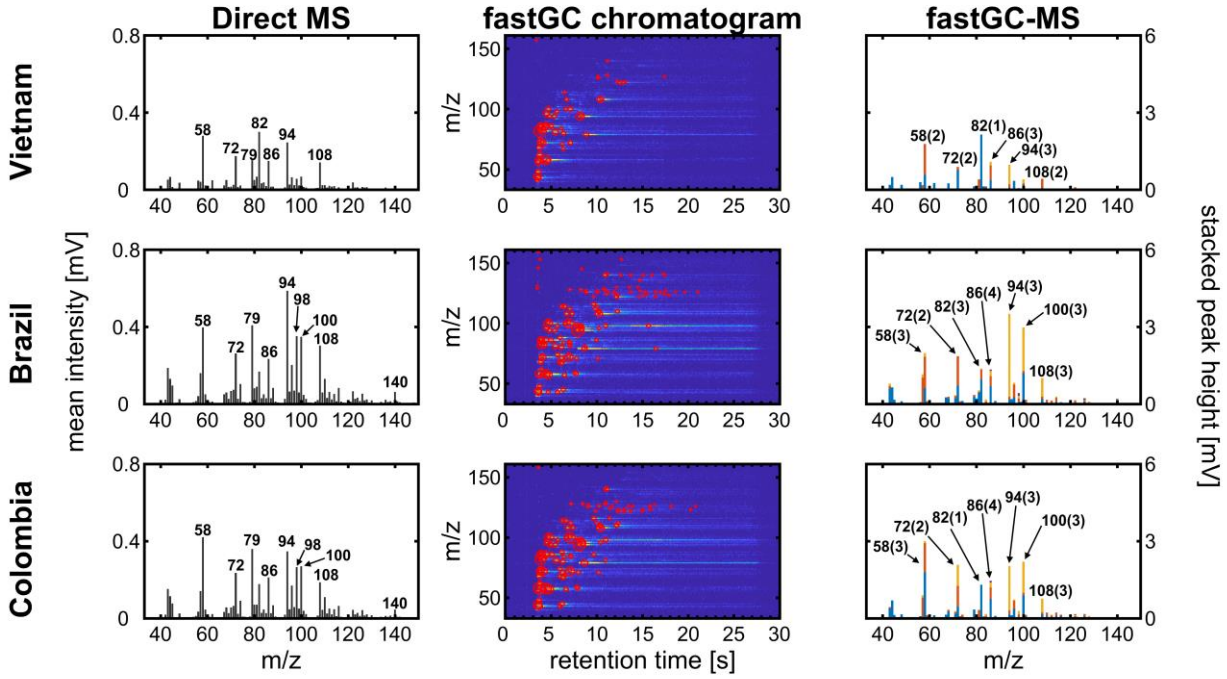

Fig. 5 Average SPI mass spectra (left column), chromatogram with peak heights highlighted as bubbles (centre column) and SPI mass spectra with stacked intensities from individual peak picking (right column) for Vietnam Robusta, Brazil Arabica and Colombia Arabica ground coffee from the same roast profile. The numbers in the mass spectra refer to the m/z and the number in brackets to the number of individual peaks detected at a nominal m/z.

retention times of the Serbian spruce needles (Fig. 4b). At later retention times, terpinoids (m/z 196), such as bornyl acetate, and sesquiterpenes (m/z 204), such as farnesene or caryophyllene become visible (Fig S2).

Roasted coffee beans. Headspace analysis of coffee beans or brewed coffee is conducted for e.g. quality control and revealing mispresentation of the coffee origin. Furthermore, the profile of VOCs released from coffee is directly link to the roast degree of the coffee and also its flavour, so attempts have been made to model e.g. roast degree and sensory attributes based on headspace analysis of coffee beans or brewed coffee[31,32]. Since different coffee cultivars release different VOC profiles during the same roast procedure[33], it offers potential for generate discrimination models in order to distinguish between different geographical origins[34].

For the mentioned applications of coffee headspace analysis, it is not entirely important to identify or even quantify the compounds of each individual peak rather than to increase the chemical space to a level enabling differentiation between coffee cultivars, origins or treatments while keeping cost and benefit balanced. For example, even not resolving isobaric compounds, DI-SPI-TOFMS has been demonstrated as a rapid analyser suitable to track rapid changes during coffee roasting with interpretable mass spectra due to its softness in ionisation[35,36].

Three different green coffees from Vietnam, Brazil and Colombia were roasted in a drum roaster receiving the same roast profile (Fig. S3), which resulted in different medium roast degrees. After degassing overnight, the roasted coffee beans were ground and analysed by fastGC-SPI-TOFMS. In the mass spectra without exploiting the chromatographic resolution, the three coffees exhibit differences in their mass spectrometric patterns (Fig. 5, left column). In particular in the lower mass range, some peaks may be unambiguously assigned to molecular structures based on knowledge from previous GC-MS studies, the ionisation threshold determined by the photon energy, the limited number of possible isomers or the strong dominance of an individual compound to a specific m/z. Such unambiguously assignments include methanethiol (m/z 48), ethanethiol (m/z 62), pyrrole (m/z 67), or pyridine (m/z 79), which are directly associated with the coffee flavour[37] or indirectly connection to other coffee properties such as antioxidant capacity or roast degree[31,38], but also caffeine (m/z 194) in the higher m/z range.

However, the two Arabica coffees from Brazil and Colombia have a high uncentred correlation coefficient of 0.98, while even between the Arabica coffees and the Robusta coffee from Vietnam we obtain good uncentred correlation coefficients of 0.86 (Brazil) and 0.89 (Colombia), respectively. The addition of fastGC gives rapid insights into the contribution of isomeric compounds to each peak (Fig. 5, centre column), which can also not be resolved at higher mass resolution. For each nominal m/z, the fastGC detects up to four individual contributions in the case of m/z 86 for Brazilian Arabica coffee, which have been linked to several carbonyl compounds, such as pentanal, butadiones, butyrolactone, methylbutanones and

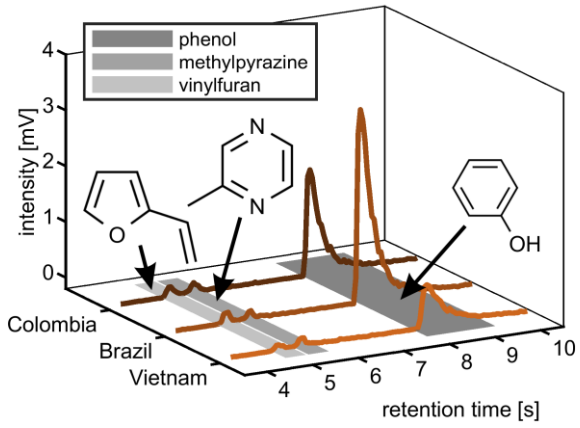

Fig. 6 Chromatograms at m/z 94 from headspace analysis of ground coffee beans f. Three peaks were tentatively assigned to vinylfuran, methylpyrazine and phenol according to identified compounds in previous studies and their relative order of elution. The Colorette values, describing the roast degree, are 106 (Vietnam), 93 (Brazil) and 81 (Colombia).

methylbutanols[35] (and references therein). Moreover, at m/z 94 we detect three peaks belonging to vinylfuran, 2-methylpyrazine and phenol (Fig. 6), which were assigned using their relative LRI and previous studies on coffee-related VOC[39,40]. 2-methylpyrazine is known for its nutty, roasted, and chocolate aroma[41] and appears with high relative abundance already in light roasts[40], whereas phenol increase toward darker roasts caused by high activation energy degradation pathway of chlorogenic acids[42]. All three coffee cultivars received the same roast profile, but ended up with different roast degrees. Therefore, the fastGC setup may be capable for offline quality control of roasted coffee.

In total, we raised the number of detected peaks from 31 (Vietnam), 47 (Brazil) and 46 (Colombia) at nominal m/z in DI-SPI-TOFMS to 53 (Vietnam), 129 (Brazil) and 106 (Colombia) individual contributions for the three coffee samples, pointing toward a higher potential in performance of fastGC-SPI-TOFMS data in chemometric prediction or discrimination models.

On-line analysis

As our fastGC setup allows rapid headspace analysis and increased confident of the result from frequently repeated measurements, its potential is even more exploited in processes with dynamic changes in VOC as shown by Fischer et al. for the case of nut roasting simulation[15]. In the following, on-line analyses with quasi-real-time resolution below 30 s are demonstrated for monitoring of the evolution of coffee roast gases and VOC emissions from the combustion of biomass.

Coffee roasting. We showcase the benefits from the addition of fastGC to SPI-TOFMS by an on-line roast gas analysis of Colombian Arabica coffee *Excelsior*. Since flavour and off-flavour formation happen fast, particularly toward the end of the roast, we shortened the GC cycle to 15 s. During the first 3 min 30 s (roasting time -2 min to 1 min 45 s) of the measurement, the sampling line was flushed with nitrogen to acquire the baseline including chemical noise and to remove possible residues of a previous roast experiment (Fig. 7). After 1 min 45 s of the start of the roast, hot roast gas was directly analysed from the drum roaster and m/z of typical products from Maillard reaction, Strecker reactions, caramelisation and thermal decomposition (pyrolysis) could be observed[36]. The most abundant compounds we observed were the furan derivatives furfuryl alcohol (m/z 98) and furfural (m/z 96) followed by two peaks for m/z 110, which likely belong to isomers of benzenediol on the one hand and methylated derivatives of furfural (methylfurfural, acetylfuran) on the other[39]. Also markers for dark roasts and also overroasts, such as pyridine (m/z 79), sharply increases toward the end of the roast, which agrees well with previous on-line analyses of coffee roast gas[33,36]. Shortly after the drop of the coffee beans, intensities generally declines and m/z below 80 reaches their baseline level within 2 min while larger VOCs are removed by purging with nitrogen.

Many attempts have been made to correlate and finally predict sensorial properties of coffee from its VOC composition by chemometric models[32,43]. Some of them were simplified to only few compounds, such as the Flavour Quality index (FQI)[37], which is was obtained from a multiple regression model and calculated by

$$FQI = 6.53 + 0.027\,[hexanal] - 0.08[vinylpyrazine] - 0.04\,[pyrrole] - 0.022[furfurylmethylketone] - 0.001[pyridine] \quad (4)$$

We modified the FQI to FQI_{mod} by removing the intercept and replace concentrations by measured peak heights, so the absolute FQI_{mod} differs from FQI, but adopt its trend. Regarding included VOC of the regression model, we note that pyrrole (m/z 67) and pyridine (m/z 79) fill unique nominal m/z with negligible interference by other compounds. At m/z 100, several isomers of the sum formula $C_6H_{12}O$ or $C_5H_8O_2$ are known, such as 2,3-pentadione, 4-methyl-2-pentanone and the so-called "coffee furanone" 2-Methyldihydro-3(2H)-furanone [39], which all may interfere with hexanal. We observe two distinct peaks in the chromatogram and recognised that hexanal and 2-methyldihydro-3(2H)-furanone have higher LRI than other carbonyl compounds at m/z 100[44]. However, the peak in the mass spectrum at m/z 101, originating from heavier isotopes, varies and appears between the theoretical values of 5.6% for $C_5H_8O_2$ and 6.7% for $C_6H_{12}O$ of the peak height at m/z 100, indicating contributions from different isomers. Nevertheless, we tentatively assigned the second peak in the chromatogram to hexanal. Moreover, we followed this approach of elution order, considering an elution order of furan < pyrazine < benzene derivatives at the same nominal m/z, also for the assignment of furfurylmethylketone and vinylpyrazine with interfering compounds guaiacol (2-methoxyphenol) and benzaldehyde, respectively, to obtain FQI_{mod}. Finally, we transferred the model from offline analysis into the time domain to investigate flavour formation during the coffee roast.

During the blank measurement with N_2, FQI_{mod} remained reasonably constant and started to fluctuate after 2 min until approximately 5 min 30 s. At this time, more m/z rise in their intensities as well as FQI_{mod} until a roast time of 7 min, referring to a lighter roast ("Cinnamon roast" to "American roast") after the first crack of the coffee beans which we heard at

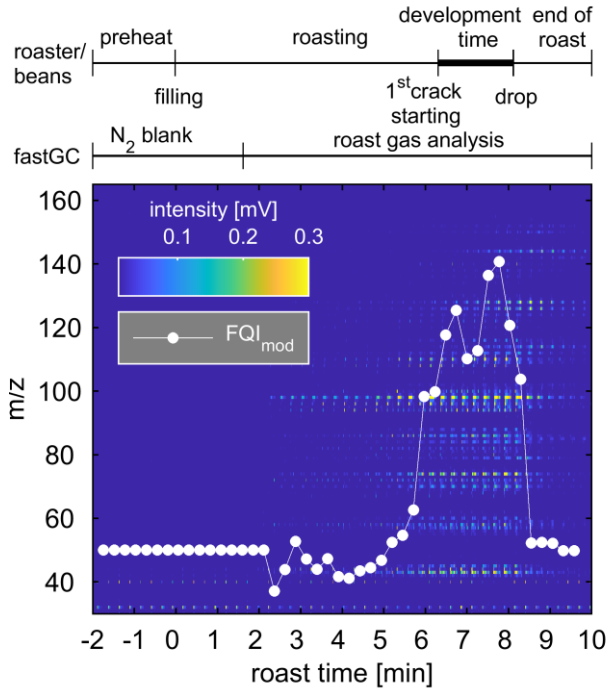

Fig. 7 Imageplot of 45 consecutive chromatograms of 15 s acquired during one roast experiment with Colombian Arabica. Peak intensities of the chromatogram are illustrated according to the colourbar. White dots represent the modified Flavour Quality Index (FQI_{mod}) comprising of hexanal (m/z 100), vinylpyrazine (m/z 106), pyrrole (m/z 67), furfurylmethylketone (m/z 124) and pyridine (m/z 79). The roast profile and Individual contributions to FQI_{mod} can be found in Fig. S3 and Fig. S4.

approximately 6min 45 s. 30 s later, FQI_{mod} reincreases to its maximum value during the roast, which still appeared before second crack of the coffee beans. Between the first and second crack, the coffee beans undergo the most significant changes in their physical and chemical properties, which is associated with flavour formation and known as "development time" [45]. The subsequent decline in FQI_{mod} may be explained by the distinct increase and higher relative contribution of pyridine, which is a common indicator for dark or overroast[36], to the intensities of individual roast gas components included in FQI_{mod} (Fig. S4). At the drop of the coffee, we obtained in fact a darker roast with a Colorette value of 81, corresponding to a medium-roasted ("City roast") coffee.

With the FQI_{mod} as proxy for the coffee flavour, we demonstrate that with shortening of the GC runtime to 15 s the fastGC-SPI-TOFMS is capable to gather the rapid the flavour formation, occurring within 2 min, from roast gas analysis of a commercial drum roaster with a realistic roast profile. Most likely, also the on-line prediction of other coffee properties, such as roast degree or antioxidant capacity, which have been modelled from photoionisation TOFMS data[38,46], would benefit from the enhanced chemical specificity of the fastGC addition.

Biomass burning. Emissions from biomass burning, either from wildfires or residential heating, are of high interest because of their direct toxicological relevance[47] and significant potential to form ground level ozone and secondary organic aerosol during atmospheric processing[48]. The combustion of biomass is dynamic in both VOC emission concentration and pattern[49], but may be represented well at a time resolution of 30 s. Consequently, we acquired 50 chromatograms during an individual open burn of twigs and foliage over 25 min.

The benefit of the increased chemical space of the analysis is demonstrated on two examples about compound identification with high confidence. For m/z 106 in pine burning emissions, we obtained varying peak heights and four separated peaks between retention times of 7 s and 11 s in each individual chromatogram (Fig. 8a-b). From previous analysis of biomass burning VOCs, we know that alkylated benzenes (C_8H_{10}: *o*-xylene, *m*-xylene, *p*-xylene, and ethylbenzene) and benzaldehyde (C_7H_6O) are present in the emissions, whereas compounds of the sum formulae $C_4H_{10}O_3$ were not detected and other possible isobars containing heteroatoms different from oxygen are unlikely to appear at such high intensities[50]. Furthermore, we assigned the peaks based on the order of elution in non-polar GC columns, which follows approximately the order of boiling points. Among these five analytes, benzaldehyde has the highest boiling point, so we assigned the peak eluting at 10.4 s. The four aromatic hydrocarbons have less difference in boiling points, which is reflected by closer LRI[24]; o- and *m*-xylene even co-elute in cGC analysis. Hence, the remaining three peaks at 7.2 s, 7.4 and 7.95 s are assigned to ethylbenzene, co-eluting *o*- and *m*-xylene, and *p*-xylene.

The second example of benefits from additional chromatographic resolution deals with the quantification of individual VOCs in wood combustion emissions by direct SPI-TOFMS in previous studies[49,51], assuming that only a single analyte contribute the to the intensity of an individual m/z. We revised this assumption for m/z 78 (benzene), 92 (toluene), 104 (styrene), 116 (indene) and 128 (naphthalene) in open burning experiments of pine branches and twigs including needles. For m/z 78, 104, 116 and 128, we got 95% contribution of the tentatively assigned VOCs. However, for m/z 78 the contribution of other compounds, likely from some minor fragmentation of methoxyphenols, may account occasionally up to 45% of its total intensity. The largest discrepancy we observed for m/z 92, to which toluene may account for less than 20% and 48% on average of the total intensity. In addition to eluting toluene at 5.4 s, further peaks appeared in the retention time range between 8 and 11 s (Fig. 8c-d), which is also covered by monoterpenes. Here, α-pinene and Δ-3-carene are the two

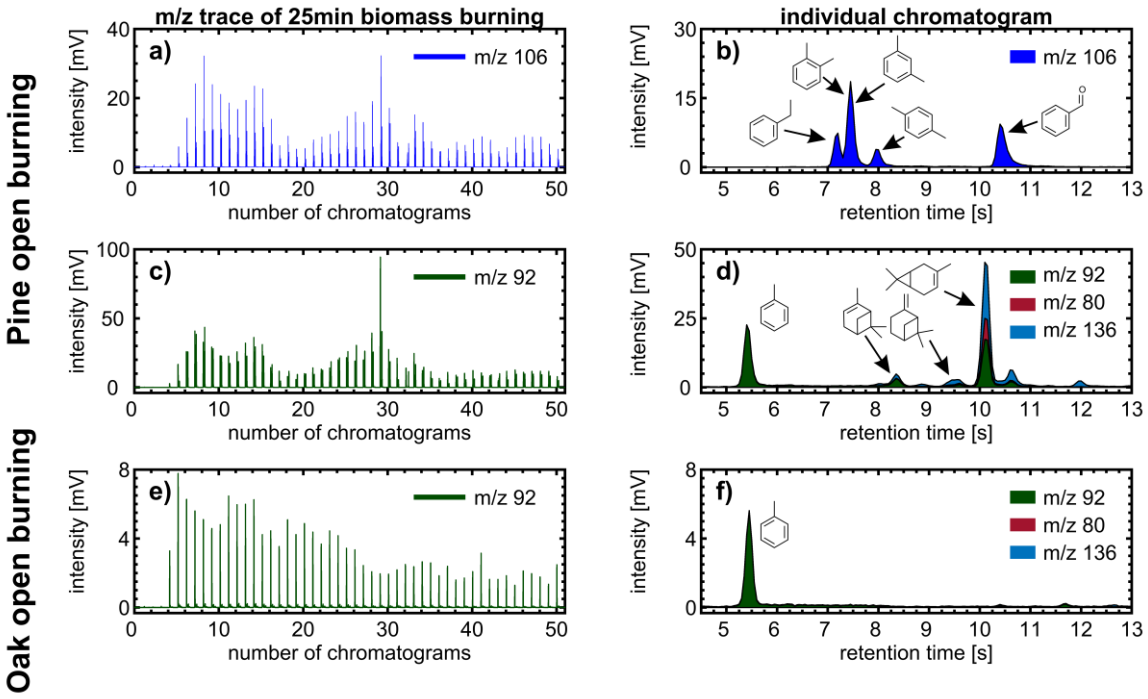

Fig. 8 Left column: 50 consecutive chromatograms of a) m/z 106 for pine open burning, c) m/z 92 for pine open burning and e) m/z 92 for oak open burning. Right column: Individual chromatograms obtained after 5 min 30 s of biomass burning. For b) m/z 106 of pine open burning, four separated peaks can be detected and assigned to ethylbenzene, co-eluting *o*- and *m*-xylene, *p*-xylene and benzaldehyde. d) The peak in m/z 92 at retention time 5.5 s belong to toluene, while peaks eluting between 8 and 12 s strongly correlate with fragments of monoterpenes. Since pine needles are rich in monoterpenes, such as Δ-3-carene, α-pinene and β-pinene, f) oak foliage and twigs with significantly lower content of monoterpenes were burned as negative control and revealed only toluene at m/z 92.

monoterpenes with high intensity of the fragment ion at m/z 92 and the most abundant monoterpene species measured in a Scots pine forest[52].

The hypothesis of monoterpenes in the Scots pine burning VOC emissions were supported by burning twigs and foliage of common oak as negative control because it contains significantly less monoterpenes than coniferous trees and consequently show significantly smaller peaks than toluene at later retention times for m/z 92 (Fig. e-f). Hence, we may expect that toluene quantification by direct SPI-TOFMS was overestimated as in Norway spruce logwood combustion in a modern masonry heater[49] and softwood pellet combustion under various pellet boiler conditions[51]. However, monoterpenes are more abundant in needles than in bark or stem wood[53] , turning the overestimation of toluene by a factor of two into similar ranges as for other quantified VOCs at m/z with assumed contribution of a single VOC.

We compared the averaged mass spectra from fastGC-SPI-TOFMS of open burning common oak and direct SPI-TOFMS measurements of beech logwood burned in a modern masonry heater[49] (Fig. S5). As expected from BTXT measurements on the trapping efficiency, the mass spectrometric pattern from fastGC-SPI-TOFMS has a bell-like shape, whereas the direct SPI-TOFMS measurement reveal declining intensities toward increasing m/z. On the one hand, small VOCs, i.e. very volatile organic compounds (VVOC), are less efficiently trapped on the modulator, but on the other hand, there is a clear benefit from fastGC of VOC speciation in the higher m/z range. For example, the fastGC is able to unravel up to 13 different individual contributions to m/z 94 (e.g. phenol and fragments from monoterpenes), separate the isobars 1-methylnaphthalene and 2-methylnaphthalene at m/z 142, and exclude significant contribution at m/z 124 from ions except the common lignin pyrolysis product 2-methoxyphenol (guaiacol)[54]. These findings were obtained only from prior knowledge about VOC emissions biomass burning, but may be extended by more systematic work on the effect of LRI from rapid temperature ramps and investigations on the fragmentation behaviour in SPI.

Conclusions

A new fastGC setup with integrated modulator sampling and detection by SPI-TOFMS was presented with its figures of merit and demonstrated in headspace and on-line analysis of samples from complementary fields. The total GC cycles of this studies last for 30 s and 15 s, thus classifying our fastGC more precisely as hyper-fast GC. Regarding LOD and precision, its performance is competitive with previously described instruments consisting of fastGC and mass spectrometric detection using soft ionisation techniques, but has advantages in chromatographic separation and GC runtime due to a highly flexible optically-heated GC unit and switch of carrier gas to helium. Additionally, the analysis benefits from the soft ionisation as co-eluting analytes of different molecular mass are separated by the mass spectrometric dimension, which does not hold for hard ionisation techniques, such as EI. On the other hand, LRIs in fastGC are fraught with higher uncertainty compared to cGC and are only usable from LRI databases to a limited extent for

compound identification, for example by considering the relative elution order of analytes. However, an implementation of quasi-simultaneous SPI/EI[55] and integration of fastGC and MS data with both hard and soft ionisation techniques may substantially enhance compound identification and classification[56].

Headspace analysis of needles from coniferous trees reveal a sufficient chromatographic separation of most abundant monoterpenes. However, also without identification by authentic standards, peaks may be assigned to common molecular indicators of the coffee roast degree in the analysis of ground roast coffee beans of different origin. As an alternative use of the short runtime for high-throughput, repeated measurements within the runtime of cGC increases the confidence of an offline measurement result.

All individual components synergise the performance of the fastGC setup in on-line analysis with a resolution of quasi-real-time. Again, coffee roasting involves complex flavour development, which may be appropriately monitored by a further total GC cycle duration of 15 s, also offering potential for more accurate real-time prediction of coffee properties relevant for human health or quality assurance. Also for the investigation of combustion emissions from solid fuels with dynamic changes in VOC emissions, our fastGC setup is capable to resolve a multiple isobaric compounds, which may be of interest for a toxicological assessment of e.g. flaming and smouldering combustion phases or an estimation of formation potential of health- and climate-relevant SOA.

Conflicts of interest

Sven Ehlert is employed by Photonion GmbH, manufacturer of the fastGC and electric modulator. Other authors declare that they have no conflict of interest.

Author contributions

H.C. and C.G. conceptualised the study. H.C. and C.G. coordinated the research planning and execution. C.G., K.S., S.E. and T.M. designed the methodology. K.S. and C.G. performed the experiments, measurements and their validation. C.G. and K.S did the data curation. C.G., K.S. and H.C. did the formal analysis. H.C. visualized the data. H.C. wrote the original manuscript draft. H.C. and R.Z. acquired the funding. All authors reviewed and edited the manuscript draft and approved its final version.

Acknowledgements

This work was supported by the German Science Foundation (DFG, grant number ZI 764/14-1) and the Helmholtz Association of German Research Centres (HGF) within the Helmholtz International Lab *aeroHEALTH* (Interlabs-0005). We thank Jan Heide for coffee roasting and comments on flavour formation.

References

1 L. Hanley and R. Zimmermann, *Anal. Chem.*, 2009, **81**, 4174–4182.
2 F. Biasioli, C. Yeretzian, T. D. Märk, J. Dewulf and H. van Langenhove, *TrAC*, 2011, **30**, 1003–1017.
3 K. Demeestere, J. Dewulf, B. de Witte and H. van Langenhove, *J. Chromatogr. A*, 2007, **1153**, 130–144.
4 H. Sonderfeld, I. R. White, I. C. A. Goodall, J. R. Hopkins, A. C. Lewis, R. Koppmann and P. S. Monks, *Atmos. Chem. Phys.*, 2016, **16**, 6303–6318.
5 M. S. Eschner, I. Selmani, T. M. Gröger and R. Zimmermann, *Anal. Chem.*, 2011, **83**, 6619–6627.
6 Q. Zhong, W. H. Steinecker and E. T. Zellers, *Analyst*, 2009, **134**, 283–293.
7 M. Zoccali, P. Q. Tranchida and L. Mondello, *TrAC-Trend. Anal. Chem.*, 2019, **118**, 444–452.
8 B. Giocastro, M. Piparo, P. Q. Tranchida and L. Mondello, *J. Sep. Sci.*, 2018, **41**, 1112–1117.
9 M. Lacko, N. Wang, K. Sovová, P. Pásztor and P. Španěl, *Atmos. Meas. Tech.*, 2019, **12**, 4965–4982.
10 H. J. Tobias and J. T. Brenna, *Analyst*, 2018, **143**, 1124–1132.
11 R. A. Di Lorenzo, V. V. Lobodin, J. Cochran, T. Kolic, S. Besevic, J. G. Sled, E. J. Reiner and K. J. Jobst, *Anal. Chim. Acta*, 2019, **1056**, 70–78.
12 N. Wang, N. Zannoni, L. Ernle, G. Bekö, P. Wargocki, M. Li, C. J. Weschler and J. Williams, *Environ. Sci. Technol.*, 2021, **55**, 149–159.
13 S. Wohlfahrt, M. Fischer, J. Varga, M.-R. Saraji-Bozorgzad, G. Matuschek, T. Denner and R. Zimmermann, *Anal. Chem.*, 2016, **88**, 640–644.
14 M. Fischer, S. Wohlfahrt, J. Varga, G. Matuschek, M. R. Saraji-Bozorgzad, T. Denner, A. Walte and R. Zimmermann, *Anal. Chem.*, 2015, **87**, 8634–8639.
15 M. Fischer, S. Wohlfahrt, J. Varga, G. Matuschek, M. R. Saraji-Bozorgzad, A. Walte, T. Denner and R. Zimmermann, *Food Anal. Methods*, 2017, **10**, 49–62.
16 M. W. Berry, M. Browne, A. N. Langville, V. P. Pauca and R. J. Plemmons, *Comp. Stat. Data Anal.*, 2007, **52**, 155–173.
17 D. Materić, M. Lanza, P. Sulzer, J. Herbig, D. Bruhn, C. Turner, N. Mason and V. Gauci, *Anal. Bioanal. Chem.*, 2015, **407**, 7757–7763.
18 M. J. Meyer, G. M. Schieffer, E. K. Moeker, J. J. Brodersen, O. F. Swenson and A. J. Borgerding, *Anal. Chem.*, 2004, **76**, 1702–1707.
19 M. S. Eschner and R. Zimmermann, *Appl. Spectrosc.*, 2011, **65**, 806–816.
20 C. Gehm, T. Streibel, J. Passig and R. Zimmermann, *Appl. Sci.*, 2018, **8**, 1617.
21 L. Fernandez, J. Yan, J. Fonollosa, J. Burgués, A. Gutierrez and S. Marco, *Front. Chem.*, 2018, **6**, 209.
22 E. Kováts, *Helv. Chim. Acta*, 1958, **41**.
23 H. van den Dool and P. D. Kratz, *J. Chromatogr. A*, 1963, **11**, 463–471.

24 W.-C. Lai and C. Song, *Fuel*, 1995, **74**, 1436–1451.

25 N. Strehmel, J. Hummel, A. Erban, K. Strassburg and J. Kopka, *J. Chromatogr. B*, 2008, **871**, 182–190.

26 C. Krill, S. Rochfort and G. Spangenberg, *Metabolites*, 2020, **10**.

27 M. Hallquist, J. C. Wenger, U. Baltensperger, Y. Rudich, D. Simpson, M. Claeys, J. Dommen, N. M. Donahue, C. George, A. H. Goldstein, J. F. Hamilton, H. Herrmann, T. Hoffmann, Y. Iinuma, M. Jang, M. E. Jenkin, J. L. Jimenez, A. Kiendler-Scharr, W. Maenhaut, G. McFiggans, T. F. Mentel, A. Monod, A. S. H. Prévôt, J. H. Seinfeld, J. D. Surratt, R. Szmigielski and J. Wildt, *Atmos. Chem. Phys.*, 2009, **9**, 5155–5236.

28 a) J. Joutsensaari, P. Yli-Pirilä, H. Korhonen, A. Arola, J. D. Blande, J. Heijari, M. Kivimäenpää, S. Mikkonen, L. Hao, P. Miettinen, P. Lyytikäinen-Saarenmaa, C. L. Faiola, A. Laaksonen and J. K. Holopainen, *Atmos. Chem. Phys.*, 2015, **15**, 12139–12157; b) N. Bertin and M. Staudt, *Oecologia*, 1996, **107**, 456–462;

29 P. H. Chowdhury, Q. He, R. Carmieli, C. Li, Y. Rudich and M. Pardo, *Environ. Sci. Technol.*, 2019, **53**, 13949–13958.

30 S. Bojovic, M. Jurc, D. Drazic, P. Pavlovic, M. Mitrovic, L. Djurdjevic, R. S. Dodd, Z. Afzal-Rafii and M. Barbero, *Trees - Struct. Funct.*, 2005, **19**, 531–538.

31 E. Liberto, M. R. Ruosi, C. Cordero, P. Rubiolo, C. Bicchi and B. Sgorbini, *J. Agric. Food Chem.*, 2013, **61**, 1652–1660.

32 C. Lindinger, D. Labbe, P. Pollien, A. Rytz, M. A. Juillerat, C. Yeretzian and I. Blank, *Anal. Chem.*, 2008, **80**, 1574–1581.

33 A. N. Gloess, A. Vietri, F. Wieland, S. Smrke, B. Schönbächler, J. A. S. López, S. Petrozzi, S. Bongers, T. Koziorowski and C. Yeretzian, *Int. J. Mass Spectrom.*, 2014, **365-366**, 324–337.

34 S. Risticevic, E. Carasek and J. Pawliszyn, *Anal. Chim. Acta*, 2008, **617**, 72–84.

35 R. Hertz-Schünemann, T. Streibel, S. Ehlert and R. Zimmermann, *Anal. Bioanal. Chem.*, 2013, **405**, 7083–7096.

36 H. Czech, C. Schepler, S. Klingbeil, S. Ehlert, J. Howell and R. Zimmermann, *J. Agric. Food Chem.*, 2016, **64**, 5223–5231.

37 R. A. Buffo and C. Cardelli-Freire, *Flav. Fragr. J.*, 2004, **19**, 99–104.

38 J. Heide, H. Czech, S. Ehlert, T. Koziorowski and R. Zimmermann, *J. Agric. Food Chem.*, 2020, **68**, 4752–4759.

39 C. Yeretzian, A. Jordan and W. Lindinger, *Int. J. Mass Spectrom.*, 2003, **223-224**, 115–139.

40 J.-K. Moon and T. Shibamoto, *J. Agric. Food Chem.*, 2009, **57**, 5823–5831.

41 N. Yang, C. Liu, X. Liu, T. K. Degn, M. Munchow and I. Fisk, *Food Chem.*, 2016, **211**, 206–214.

42 R. Dorfner, T. Ferge, C. Yeretzian, A. Kettrup and R. Zimmermann, *Anal. Chem.*, 2004, **76**, 1386–1402.

43 a) M. R. Baqueta, A. Coqueiro and P. Valderrama, *J. Food Sci.*, 2019, **84**, 1247–1255; b) D. Bressanello, E. Liberto, C. Cordero, B. Sgorbini, P. Rubiolo, G. Pellegrino, M. R. Ruosi and C. Bicchi, *J. Agric. Food Chem.*, 2018, **66**, 7096–7109;

44 J. M. Ames, R. C. Guy and G. J. Kipping, *J. Agric. Food Chem.*, 2001, **49**, 4315–4323.

45 M. Münchow, J. Alstrup, I. Steen and D. Giacalone, *Beverages*, 2020, **6**, 29.

46 H. Czech, J. Heide, S. Ehlert, T. Koziorowski and R. Zimmermann, *Foods*, 2020, **9**, 627–650.

47 a) T. Kanashova, O. Sippula, S. Oeder, T. Streibel, J. Passig, H. Czech, T. Kaoma, S. C. Sapcariu, M. Dilger, H.-R. Paur, C. Schlager, S. Mülhopt, C. Weiss, C. Schmidt-Weber, C. Traidl-Hoffmann, B. Michalke, T. Krebs, E. Karg, G. Jakobi, S. Scholtes, J. Schnelle-Kreis, J. Orasche, L. Müller, A. Reda, C. Rüger, A. Neumann, G. Abbaszade, C. Radischat, C. Hiller, J. Grigonyte, M. Kortelainen, K. Kuuspalo, H. Lamberg, J. Leskinen, I. Nuutinen, T. Torvela, J. Tissari, P. I. Jalava, S. Kasurinen, O. Uski, M.-R. Hirvonen, J. Buters, G. Dittmar, J. Jokiniemi and R. Zimmermann, *J. Mol. Clin. Med.*, 2018, **1**, 23–35; b) Y. H. Kim, S. H. Warren, Q. T. Krantz, C. King, R. Jaskot, W. T. Preston, B. J. George, M. D. Hays, M. S. Landis, M. Higuchi, D. M. DeMarini and M. I. Gilmour, *Environ. Health Perspect.*, 2018, **126**, 17011;

48 a) J. B. Gilman, B. M. Lerner, W. C. Kuster, P. D. Goldan, C. Warneke, P. R. Veres, J. M. Roberts, J. A. de Gouw, I. R. Burling and R. J. Yokelson, *Atmos. Chem. Phys.*, 2015, **15**, 13915–13938; b) A. Hartikainen, P. Tiitta, M. Ihalainen, P. Yli-Pirilä, J. Orasche, H. Czech, M. Kortelainen, H. Lamberg, H. Suhonen, H. Koponen, L. Hao, R. Zimmermann, J. Jokiniemi, J. Tissari and O. Sippula, *Atmos. Chem. Phys.*, 2020, **20**, 6357–6378;

49 H. Czech, O. Sippula, M. Kortelainen, J. Tissari, C. Radischat, J. Passig, T. Streibel, J. Jokiniemi and R. Zimmermann, *Fuel*, 2016, **177**, 334–342.

50 S. K. Akagi, R. J. Yokelson, C. Wiedinmyer, M. J. Alvarado, J. S. Reid, T. Karl, J. D. Crounse and P. O. Wennberg, *Atmos. Chem. Phys.*, 2011, **11**, 4039–4072.

51 H. Czech, S. M. Pieber, P. Tiitta, O. Sippula, M. Kortelainen, H. Lamberg, J. Grigonyte, T. Streibel, A. S. H. Prévôt, J. Jokiniemi and R. Zimmermann, *Atmos. Environ.*, 2017, **158**, 236–245.

52 R. Janson, *J. Atmos. Chem*, 1992, **14**, 385–394.

53 U. Bufler and Seufert, G., Jüttner, F., *Environ. Pollut.*, 1990, **68**, 367–375.

54 M. Elsasser, C. Busch, J. Orasche, C. Schön, H. Hartmann, J. Schnelle-Kreis and R. Zimmermann, *Energy Fuels*, 2013, **27**, 4959–4968.

55 M. S. Eschner, T. M. Gröger, T. Horvath, M. Gonin and R. Zimmermann, *Anal. Chem.*, 2011, **83**, 3865–3872.

56 D. R. Worton, M. Decker, G. Isaacman-VanWertz, A. W. H. Chan, K. R. Wilson and A. H. Goldstein, *Analyst*, 2017, **142**, 2395–2403.